Interfacial Nanoparticle Complexation of Oppositely Charged Nanocelluloses into Functional Filaments with Conductive, Drug Release or Antimicrobial Property

Kaitao Zhang[1], Sry D. Hujaya[1], Topias Järvinen[2], Panpan Li[1], Topias Kauhanen[3], Mysore V. Tejesvi[3,4], Krisztian Kordas[2], Henrikki Liimatainen[1]*

[1]Fibre and Particle Engineering Research Unit, Faculty of Technology, University of Oulu, P.O. Box 4300, FI-90014, Finland

[2]Microelectronics Research Unit, Faculty of Information Technology and Electrical Engineering, University of Oulu

[3]Department of Ecology and Genetics, PO Box 3000, University of Oulu

[4]Chain Antimicrobials Ltd, Teknologiantie 2, FI-90590, Oulu, Finland

KEYWORDS: Self-assembly, nanocellulose, interfacial complexation, filament, biomedical application, electrostatic interactions

ABSTRACT

Construction of colloidal nanoparticles into advanced functional nanocomposites and hybrids with pre-designed hierarchical structure and high-performance is attractive, especially for natural biological nanomaterials, such as proteins and polysaccharides. Herein, a simple and sustainable approach called interfacial nanoparticle complexation (INC) was applied to construct diverse functional (conductive, drug-loaded or antimicrobial) nanocomposite filaments from oppositely charged colloidal nanocelluloses. By incorporating different additives during the INC process, including multi-walled carbon nanotube, an antitumor drug (doxorubicin hydrochloride, DOX), and metal (silver) nanoparticles (Ag NPs), high-performance functional continuous filaments were synthesized and their potential applications in electronics, drug delivery and antimicrobial materials were investigated, respectively. This novel INC method based on charged colloidal nanoparticles opens new avenues for building various functional filaments for a diversity of end-uses.

INTRODUCTION

After billions of years of evolution, nature has developed outstanding-performance biological materials, such as bone, tooth, wood, and mollusk shell.[1, 2] The intimate assembly of the micro- and/or nanoscopic scales biological building blocks always result in sophisticated hierarchical structures with a variety of excellent mechanical, optical, and electrical properties.[3-9] These biological materials not only are generally synthesized and processed via a green way and in mild conditions (e.g. in aqueous circumstance and at room temperature), but also inspire materials scientists to design the sustainable structural composites.[4, 10] Cellulose, as one of the most versatile and widely found biopolymers in nature, has been used by humans for centuries. Nanocellulose (usually refers to cellulose nanocrystal, cellulose nanofibrils or bacterial nanocellulose) is nanostructured cellulose with at least one dimension <100 nm,

which could be isolated from diverse and sustainable cellulosic materials such as wood pulp, cotton linters, tunicin, and bacterial cellulose.[11] Except for the properties for which cellulose is known, including low density, nontoxicity, and high biodegradability, nanocellulose also holds many unique and appealing features (such as high mechanical strength, reinforcing capabilities, and tunable self-assembling property) owing to its nano-scaled structure, high surface reactivity, and high degree of crystallinity.[12] By proper modification, various charged groups such as sulfate, carboxylate, sulfonate, quaternary ammonium and phosphonate groups, can be attached to the surface of nanocellulose [13-15] and act a crucial role in directing the assembly of nanocelluloses.[16-22]

Self-assembly of oppositely charged molecules, polymers or colloids to different hierarchically structured materials such as layer-by-layer films,[23, 24] polyelectrolyte complex membranes (PEMs),[25] polyionic complex particles,[26] microcapsules,[27] hydrogels[28] and interfacial polyelectrolyte complexation (IPC) filaments[29-34] has been extensively investigated in recent decades. Owing to their high biocompatibility, excellent biodegradability, low toxicity, and energy-efficient production process, these materials have been widely used in numerous technological and scientific fields such as pharmacy, biomaterials, biomedicine and cosmetics.[35-40] Recently, we found that a system consisting only of oppositely charged nanoparticles could be applied to form hierarchical filaments via a novel phenomenon termed as interfacial nanoparticle complexation (INC).[41] The INC filaments were simply fabricated by interfacial complexation of two oppositely charged colloidal nanocellulose (NC) particles in aqueous suspension at room temperature. This straightforward, bottom-up process not only might provide a new route to fabricate continuous filaments from oppositely charged nanoparticles pairs (e.g. cationic chitin or protein nanofibrils with anionic graphene oxide), but more importantly, may also allow for the integration of multiple functionalities into the self-assembled filaments. Moreover, we believe that the utilizing of the intrinsic properties of the nanoparticles (such as the crystallinity of nanocellulose or

nanochitin and the electrical conductivity of reduced graphene oxide), filaments with other advanced properties such as higher tensile strength or electrical conductive could be obtained in future.

In this report, a new type of nanocellulose based INC filament was firstly fabricated by two oppositely charged nanocelluloses. Cationic cellulose nanocrystals (AH-CNC) were synthesized by Schiff reaction between di-aldehyde cellulose and aminoguanidine hydrochloride in deep eutectic solvent by our previously reported method (see the chemical structure in Supporting Information (SI) in Figure S1).[42] Anionic TEMPO-oxidized cellulose nanofibers (TO-CNF) were prepared by 2,2,6,6-tetramethylpiperidinyl-1-oxy radical (TEMPO) oxidation method. By incorporating carboxylated multi-walled carbon nanotubes (CMWCNTs), an antitumor drug (doxorubicin hydrochloride, DOX), or metal (silver) nanoparticles (Ag NPs) into the self-assembled microfibers, various functional (conductive, drug loaded and anti-microbial) INC filaments were designed and their potential applications in the fields of flexible electronics, drug delivery and antimicrobial materials were investigated, respectively.

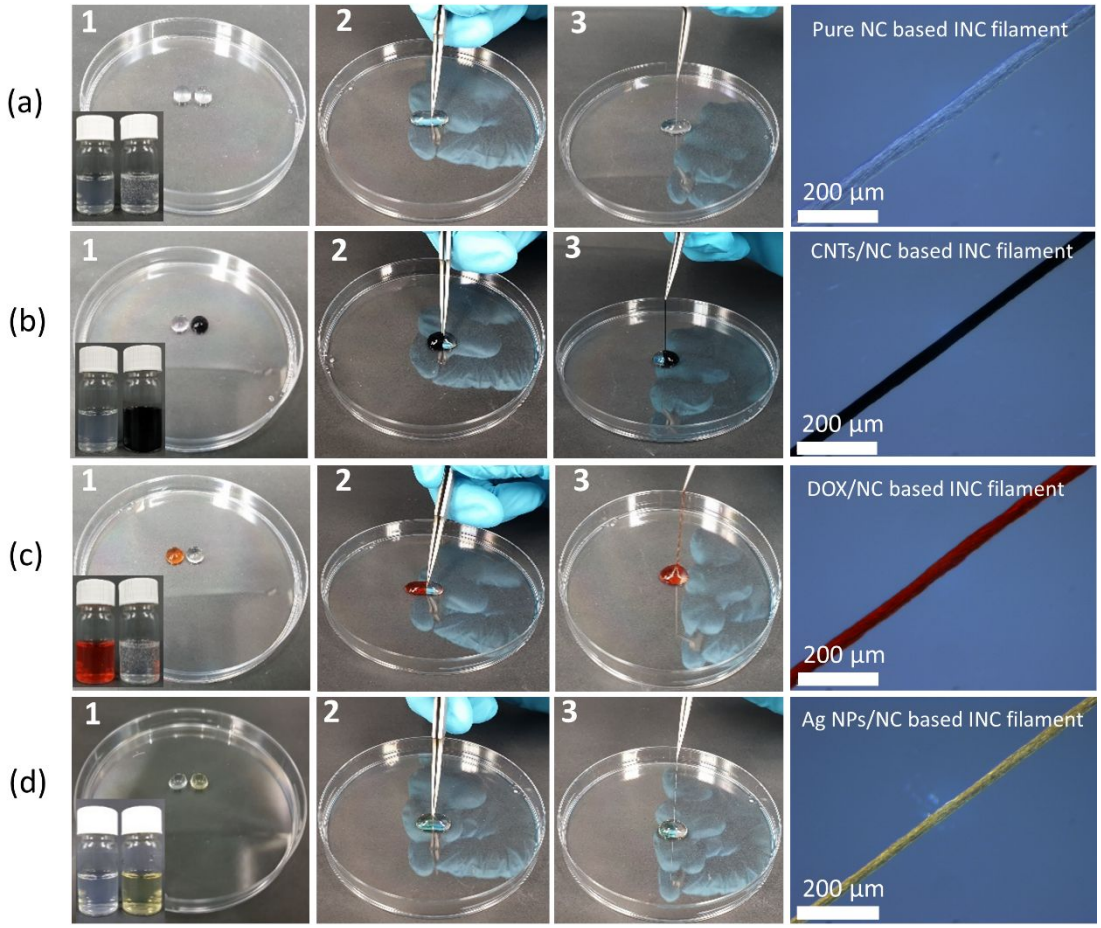

Figure 1. Digital photographs of the drawing process of each INC filament and corresponding optical microscope images of the dried INC filaments: (a) anionic suspension: 0.5 wt% TO-CNF; cationic suspension: 0.5 wt% AH-CNC; (b) anionic suspension: 0.5 wt% TO-CNF with 0.2 wt% CMWCNTs; cationic suspension: 0.5 wt% AH-CNC; (c) anionic suspension: 0.5 wt% TO-CNF; cationic suspension: 0.5 wt% AH-CNC with 200 µg/mL DOX; (d) anionic suspension: 0.4 wt% TO-CNF with 0.005 mmol/mL Ag NPs; cationic suspension: 0.5 wt% AH-CNC.

EXPERIMENTAL SECTION

Materials. Bleached birch (Betula pendula) chemical wood pulp obtained in dry sheets was used as cellulose raw material. The properties of birch pulp were analyzed in a previous study.[43] 2,2,6,6-tetramethylpiperidinyl-1-oxy radical (TEMPO), sodium bromide (NaBr), lithium chloride (LiCl), sodium

hypochlorite solution (NaClO, 15 wt%), sodium chlorite ($NaClO_2$), sodium periodate ($NaIO_4$), Dulbecco's Modified Eagle's Medium (DMEM), NIH3T3 Cell and silver dispersion (10 nm particle size, 0.02 mg/mL in aqueous citrate buffer) were obtained from Sigma–Aldrich (Finland) and used without further purification. Doxorubicin hydrochloride (DOX) and aminoguanidine hydrochloride (>98%) were purchased from Tokyo Chemicals Industry (TCI Chemicals, Japan). Carboxlyated multi-walled carbon nanotube powder (CMWCNTs) was purchased from TimeNano (Chengdu, China). PBS (Phosphate Buffered Saline) and DPBS (Dulbecco's Phosphate Buffered Saline) buffer were prepared by dissolving NaCl, KCl, $KH_2PO_4 \cdot H_2O$ and $Na_2HPO_4 \cdot 2H_2O$ in the appropriate amounts in deionized water and by adjusting the pH using HCl or NaOH. Acetate buffer saline (ABS) pH 4 were prepared by mixing 0.1 M acetic acid glacial and 0.1 M sodium acetate in the appropriate amounts in deionized water and by adjusting the pH using HCl or NaOH.

Fabrications of different nanocellulose (NC) based interfacial nanoparticle complexation (INC) filaments. CMWCNTs and Ag NPs were mixed with anionic TO-CNF, respectively, and cationic DOX was mixed with cationic AH-CNC. The detailed protocols used for the preparation of these functional INC filaments can be found in supporting information. Figure 1 shows the drawing process of INC filaments. One 100 μL of droplet each from two oppositely charged aqueous nanocellulose suspensions was pipetted adjacent to the other on a plastic Petri dish. An interface complex film formed immediately when a pair of tweezers was plunged into the two droplets to make the two droplets into contact. The interface film acts as a viscous barrier, which prevents the mixing of the dispersions. Nanocellulose (NC) based INC filament was drawn vertically from the formed interface complex film by the tweezers. In order to obtain homogeneous continuous filaments, all the INC filaments were drawn by a tensile testing machine with a constant rate of 30 mm/min (SI Figure S2). The obtained wet INC filaments were wrapped on the glass rod and dried at room temperature. The NC based INC filament containing

CMWCNTs, DOX or Ag NPs was coded as CNTs/NC based INC filament, DOX/NC based INC filament, and Ag NPs/NC based INC filament, respectively.

Physicochemical Characterization. The cationic group content of AH-CNC and the composition of the pure nanocellulose based filaments were calculated directly from the nitrogen content of the product as determined by an elemental analyzer (CHNS/O 2400 Series II, PerkinElmer, USA). The samples sputtered with platinum were examined using a field emission scanning electron microscopy (FESEM, Zeiss Sigma HD VP, Oberkochen, Germany) at 0.5 kV acceleration voltage. The elemental mapping was performed using Energy Dispersive Spectroscopy (EDS) manufactured by Bruker and the sample for EDS were coated by carbon. The chemical characterization of nanocelluloses and the formed filaments were carried out using diffuse reflectance infrared Fourier transform (DRIFT). The spectra were recorded on a Bruker Vertex 80v spectrometer (USA) in the 800–4000 cm^{-1} range with 2 cm^{-1} resolution. Electrical conductivities of CNT-incorporated nanocellulose based filaments were measured using a two-point probe setup (Keithley 2636A sourcemeter). Silver paste was painted at the end of the filament and used as a contact point. The conductivity was calculated from the current–voltage (I–V) curve. When calculating the conductivity, the cross-section of filament was regarded as a perfect round shape. The length and diameter of the filaments were measured by optical microscopy (Leica MZ6 equipped with a Leica DFC420 camera). Each sample was repeated six times, and the values with large errors were excluded. The mechanical properties of the drawn filaments were studied using a universal testing machine (Zwick D0724587, Switzerland) equipped with a 200 N load cell. The fabricated cellulose filaments were glued on paper frames before being tested to avoid fiber slippage, and were then mounted on the clamps. All the samples were tested at a strain rate of 5 mm/min at room temperature and a gauge length of 20 mm using a pre-force of 0.01 N until breakage. Five replicates for each material were tested

and all samples were placed at a relative humidity of 50% at a temperature of 22°C for at least one day prior to the testing.

In-vitro DOX release studies. DOX release profiles were studied by immersing five 70 cm DOX loaded filaments into 2 mL of release medium (either PBS buffer pH 7.4 or ABS pH 4) and incubating at 37 °C. At predetermined time intervals, 1 mL of medium from each vial was collected and 1 mL of fresh medium was replaced. The amount of DOX in collected medium was determined using a UV spectrophotometer (UV-1800, Shimadzu, Japan) for the absorbance values at the λ_{max} of doxorubicin (480 nm). Each release study experiment was run in triplicate.

In-vitro cell biocompatibility and efficacy studies. NIH3T3 cells were grown in DMEM containing 4.5 g/L glucose and GlutaMAXTM (Gibco) supplemented with 1% (v/v) PennStrepp (Sigma-Aldrich) and 10% (v/v) fetal bovine serum (Gibco). Cells were cultured at 37 °C, in a 5% CO_2 incubator, trypsinized at about 90% confluency, and split at 1:4 or 1:5 ratio. To obtain a non-woven fabric for seeding cells, six filaments of 70 cm in length were bonded into scaffolds using a hydro-entanglement process. Entanglement of the fibers led to fibrous and porous scaffolds that retained good shape stability in water. Then, hydroentangled nanocellulose based INC filament (HNF) scaffolds were sterilized in 70% ethanol for 30 min, washed twice with DPBS and finally with complete DMEM for preconditioning. NIH3T3 cells were then seeded on top of the conditioned scaffolds at a density of 100 000 cells/scaffold and left to attach in the incubator (37 °C, 5% CO_2) for 2 h, after which more complete medium was added. Cells grown on tissue culture-treated polystyrene (TCPS) on approximately the same surface area were regarded as positive controls. Cells were cultured in the incubator for a total of 4 days. On day 2 of culture, each well was added with 10X AlamarBlue (Invitrogen) at 10% v/v and incubated for 6 h. An aliquot of conditioned AlamarBlue-containing medium was collected from each well for measurements of metabolic activity on day 2 while the rest of the cells were cultured further. Since the AlamarBlue is

nontoxic to cells, it can be left in the culture media to follow growth at latter time points. After a total of 4 days of culture, another aliquot of conditioned AlamarBlue-containing medium was collected and measured. The fluorescence intensity of resorufin (i.e. metabolically-reduced resazurin) was then recorded using a Victor3 plate reader (PerkinElmer). All fluorescence intensities recorded were corrected by subtracting each value with the average of each respective no-cell control wells. All cell experiments were carried out in triplicates.

Fluorescence imaging of live cells. After one day of culture, cell-containing scaffolds were washed twice with DPBS, stained with Hoechst 33342 (Invitrogen) for live cells and propidium iodide (PI, Invitrogen) for dead cells for 10 min at RT and washed another two times with DPBS. Samples without DOX were stained with both Hoechst and PI while samples with DOX were stained only with Hoechst due to the overlapping excitation and emission spectra of PI and DOX. Fluorescence imaging was performed on an Axio Scope.A1 (Zeiss) upright fluorescence microscope equipped with a water immersion objective at 40X magnification (Olympus). Fluorescence of DOX was imaged using the GFP channel.

Statistical analysis. Data were analyzed and plotted with the GraphPad Prism version 6.01 software. All data represent means ± standard deviation. Multiple comparisons between treatment types within the same treatment duration were performed based on the one-way analysis of variance (ANOVA), while statistical significance analysis between any two sets of data was performed based on the two-tailed, paired or unpaired Student t-test, and differences were deemed significant when $p < 0.05$. P values may range from way below or above 0.05 or slightly larger than 0.05 as discussed in the text when necessary.

Antimicrobial testing. The antibacterial activity of the fabricated filaments was tested against *Staphylococcus aureus* (*S.aureas*, Gram positive) and *Escherichia coli* (*E.coli*, Gram negative). Ag NPs doped INC filaments disc was prepared by condensing five 70 cm filaments together. The fabricated

discs were placed on Mueller Hinton broth agar (Merk, Darmstadt, Germany) plates, which had been previously seeded with 0.2 mL of inoculums containing approximately 10^5 to 10^6 CFU/mL of E. coli or S.aureas. The plates were then incubated at 37 °C for 24 h.

RESULTS AND DISCUSSION

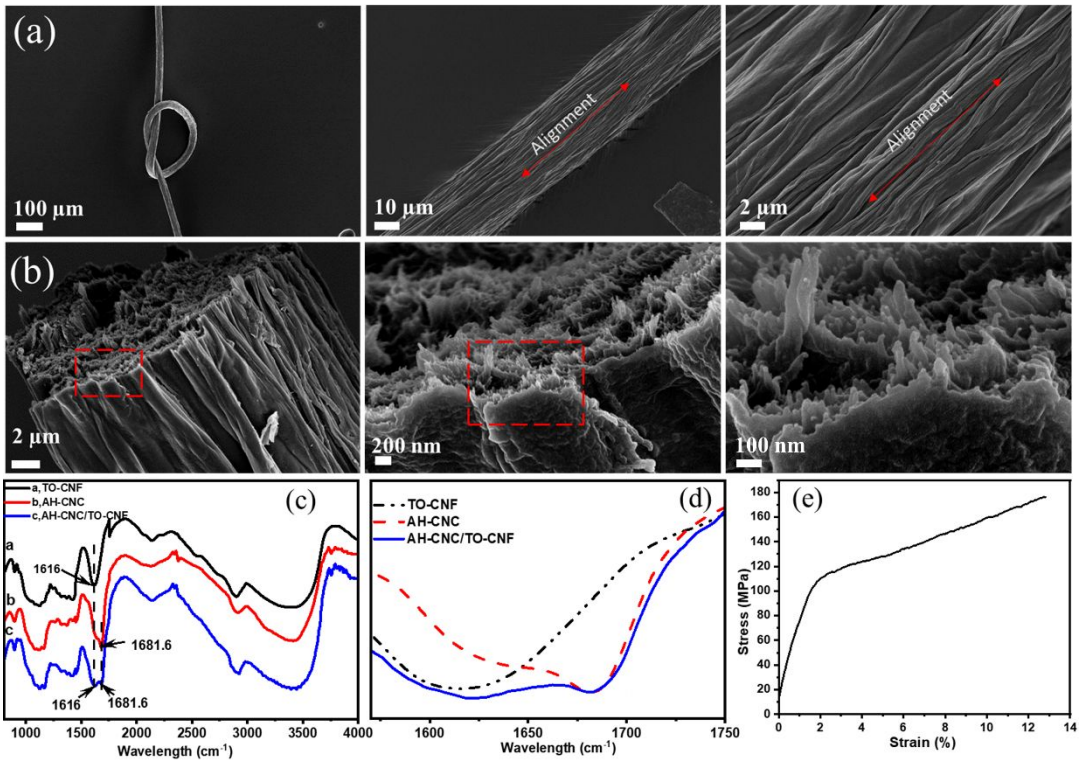

Figure 2. Scanning electron microscopy (SEM) images of (a) longitudinal direction and (b) cross-sectional fracture of pure nanocellulose based INC filaments. The DRIFT spectra (c) and typical peaks (d) of the formed pure nanocellulose based INC filaments and its respective components; (e) a typical stress-strain curve of the fabricated filaments using 0.5% TO-CNF and 0.5% AH-CNC.

Pure NC based INC filament was successfully fabricated by interfacial nanoparticle complexation of positively charged AH-CNC with negatively charged TO-CNF. AH-CNC (129±36 nm in length and 7±3 nm in width, see TEM image in SI Figure S3) with a cationic charged density of 2.3 mmol/g was used

as the positively charged component. TO-CNF (172 to 958 nm in length and 5±2 nm in width, see TEM image in SI Figure S3) with an anionic charge density of 1.6 mmol/g was in turn used as the negatively charged component. The feasibility of drawing the NC based INC filaments from various concentration of AH-CNC and TO-CNF are presented in Table S1 in supporting information. Figure 2 shows SEM images of formed pure NC based INC filaments. The formed filaments were flexible and could be knotted to form a loop. Parallel sub-micron fibers could be observed aligned along the longitudinal axis of the INC filament (Figure 2a). Moreover, nano-sized fibers (NFs) were also observed in a nearly circular cross-section area of the filaments (Figure 2b, SI Figure S4), showing a hierarchical structure consistent with our previous results.[34] We deduced that these nanofibers were formed via interfacial nanoparticle complexation of the oppositely charged nanocelluloses, since their average diameter (31±7 nm) was larger than that of constituent individual nanocellulose.[41] Nitrogen was detected in the fabricated filament by elemental analysis, indicating that AH-CNC was successfully incorporated into the cellulosic filament. The AH-CNC content in the formed filament was determined to be 45.4%. The DRIFT spectra of fabricated nanocellulose based filament (Figure 2c and d) presented the two typical peaks in cationic nanocellulose (1681.6 cm^{-1}, corresponding carbon–nitrogen double bond in AH-CNC) and anionic nanocellulose (1616 cm^{-1}, corresponding C=O stretching frequency of sodium carboxylate in TO-CNF). A typical stress-strain curve of the fabricated filaments using 0.5% TO-CNF and 0.5% AH-CNC is shown in Figure 2e. The tensile strength of the formed INC filament can reach 178 ± 18 MPa with Young's modulus of 8.4±1.5 GPa and strain of 13.5±3%.

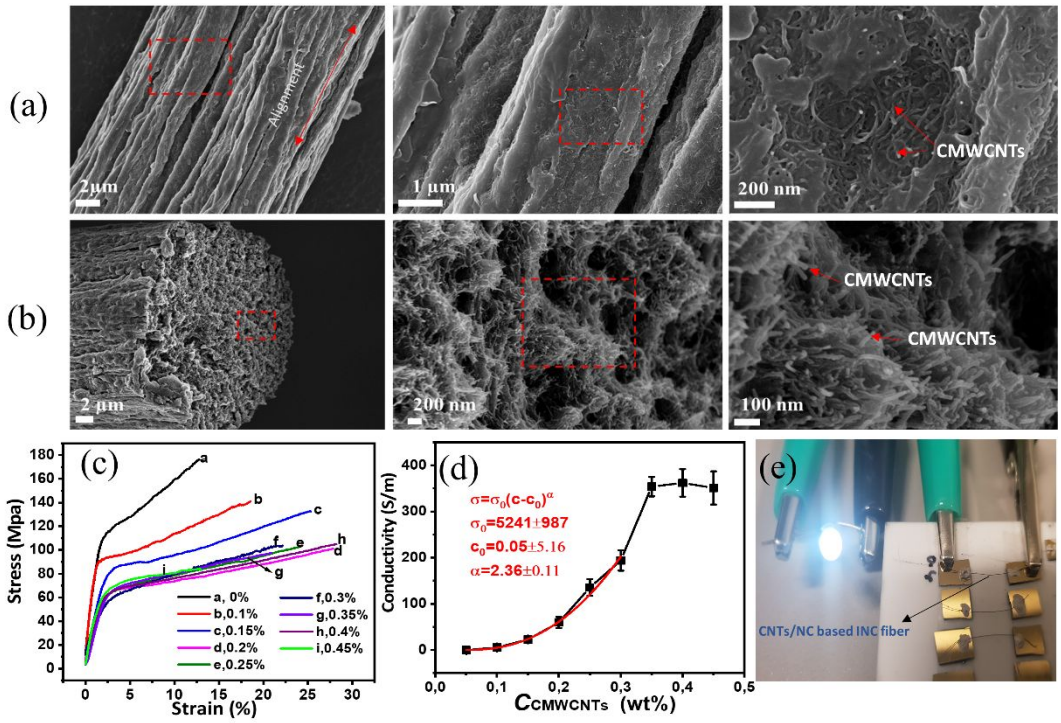

Figure 3. SEM images of (a) longitudinal and (b) cross-sectional fracture of CMWCNTs incorporated INC filaments. (c) Typical stress-strain curves and (d) electrical conductivity of INC filaments fabricated using different CMWCNTs concentrations in TO-CNF dispersion. (e) Photograph showing a light emitting diode (LED) operating using an individual CMWCNTs incorporated INC filament fabricated by 0.35 wt% CMWCNTs in TO-CNF suspension (47.3 wt% CMWCNTs, 45.5 μm diameter).

Table 1. Characteristics of fabricated CMWCNTs-incorporated nanocellulose based filament.[a]

$C_{CMWCNTs}$[b] (wt%)	Ultimate tensile strength (MPa)	Strain at break (%)	Young's modulus (GPa)	Electrical conductivity (S/m)
0	178 ± 18	8 ±2	8±2	
0.1	141±13	20±4	5±2	6±3
0.15	126±7	28±4	3.7±1.0	23±4
0.2	104±5	29±6	3.6±0.7	60±12
0.25	109±8	25±3	3.1±0.9	135±20
0.3	108±5	24±3	4.1±0.6	194±30

0.35	101±5	29±7	2.5±0.6	354±30
0.4	103±13	27±4	3.0±0.4	362±30
0.45	83±13	13±6	4.0±0.5	351±40

a, For all samples, anionic TO-CNF (0.5 wt%) was used to disperse CMWCNTs and the filaments were formed with the mixture suspensions of TO-CNC/CMWCNTs and 0.5wt% cationic AH-CNC. *b,* $C_{CMWCNTs}$ represents the concentration of CWCNTs in the TO-CNF dispersion.

It was reported that nanocellulose could disperse carbon nanotubes (both single and multi-walled) in aqueous solvents.[44, 45] Conductive fiber, serving as an important component in wearable electronics, has gained tremendous attention by virtue of their high flexibility, knittability, and lightweight.[46] The production of nanocellulose/CNTs filaments have been reported based on this strategy using several methods such as wet-spinning,[47] flow-focusing,[48] and 3D-Printing.[46] Here, in order to obtain conductive INC filaments, TO-CNF aqueous suspension with a concentration of 0.5wt% was used as a dispersant to prepare TO-CNF/CMWCNTs suspensions, the obtained TO-CNF/CNTs mixture with different CMWCNTs concentration was then applied as the negative component to draw the CMWCNTs doped nanocellulose (CNTs/NC) based INC filaments with 0.5 wt% AH-CNC (Figure 1b). The mixture suspensions of CMWCNTs (from 0.1 to 0.45 wt%) dispersed with TO-CNF could stay stable for several months. It is reported that nanocellulose with high surface charge density can be used as an efficient dispersant for hydrophobic carbon nanotubes to form nanocomposites. [46, 48] The interaction between the charged nanocellulose and the carbon nanotubes is governed by conductive sp^2 carbon lattice, and the CNT and nanocellullose form associated structures that are electrostatically stabilized through the charges of the nanocellullose (i.e. electrostatic repulsion).[44] Thus, we assumed that the electrostatic interaction would occur between the positively charged nanocellulose (AH-CNC) and associated structures of anionic nanocellulose (TO-CNF) and CMWCNTs. Figure 3a and b show the SEM images of longitudinal and cross-section area of the obtained filaments (more SEM images could be found in SI Figure S5). A nervation/veining pattern similar to pure nanocellulose INC filaments was observed on the

surface CNTs/NC based filaments. In addition, CMWCNTs were found on the surface of the formed INC filament. Some long and randomly arranged CMWCNTs were also observed in the cross-section area even though they have a similar diameter (20 nm in diameter for CMWCNTs) with formed cellulosic nano-sized fibers in the cross-section area. The stress-strain curve and electrical conductivity of the CNTs/NC based INC filaments are depicted in Figure 3c, d (detailed data could be found in Table S2 in supporting information). With an increase of the content of CMWCNTs in TO-CNF suspension, both tensile strengths and Young's modulus of the resulting filaments were reduced. This decrease is probably ascribed to the insufficient interaction between the oppositely charged nanocelluloses due to the incorporation of CMWCNTs. On the contrary, the maximum strain of the formed filaments increased as a function of CMWCNTs in TO-CNF suspension. The electrical conductivity of the formed CNTs/NC based INC filaments increased with increasing CMWCNTs concentration and could reach up to 392 S/m with a concentration of 0.4% CMWCNTs (the content of CMWCNTs in formed INC filament fabricated by 0.4 % CNTs in TO-CNF suspension was 59.1 wt%). The filler concentration c dependent conductivity σ of the composite follows well the power law of percolating networks: $\sigma = \sigma_0(c-c_0)^{\alpha}$, where σ_0 and c_0 are the threshold conductivity and concentration, and α is the critical exponent describing the dimensionality of the percolation. The value of α extracted from the data by fitting at low filler concentrations gives 2.36±0.11, which is quite close to the theoretical value (α=2) for 3-dimensional percolating networks. CNTs/NC based INC filament, which was mounted on a conductive substrate by silver paste and connected to a 1.5 V battery, could conduct sufficiently high current to operate a LED (Figure 3e). It is envisaged that CNTs/NC based INC filament with a higher electrical conductivity could be obtained by applying single walled CNTs. Moreover, various other 1D or 2D hydrophobic fillers (e.g., boron nitride nanotubes and nanosheets, SiC, and graphene) can be dispersed into nanocellulose suspensions,[49, 50] which also could be utilized to engineer hydrophobic fillers/NC composite filament by the INC technique.

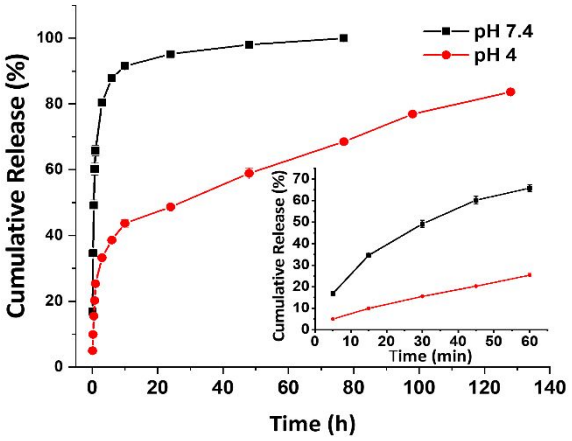

Figure 4. Cumulative release profiles of DOX-loaded NC based INC filaments in different pH values at 37 °C. The inset shows the cumulative drug release in the first one hour.

As INC filament was formed in aqueous suspensions at room temperature, the INC filaments show high potential in biomedical application such as drug delivery and tissue engineering.[51-53] To demonstrate the feasibility of utilizing NC based INC filament as a matrix for drug release, an cationic antitumor drug (DOX, doxorubicin hydrochloride) as a model was encapsulated into the nanocellulose based INC filaments. Cationic DOX was firstly mixed with 0.5 wt% cationic AH-CNC suspension resulting in a mixture dispersion with a concentration of 200 μg/mL DOX. The mixture was then used as a positively charged component to fabricate DOX-loaded NC (DOX/NC) based INC filaments (Figure 1c). Positively charged DOX could be trapped into the filament owning to its electrostatic interaction with negatively charged TO-CNF. During the DOX/nanocellulose INC fiber formation, not only the positively charged nanocellulose but also the DOX interacts with the negatively charged nanocellulose, forming the DOX loaded INC fibers. However, pure DOX could not form filaments with anionic nanocellulose owning to the low molecular weight of DOX. The DOX loading efficiency into the INC filaments was determined to be 83±1% by measuring the total amount of residual DOX in the combined droplets after thirty filaments drawing (see details in SI). Figure 4 depicts the cumulative release profiles of DOX at different pH media. Obviously, the drug release was influenced by pH value of the medium solutions, where DOX

released faster in physiological pH (pH 7.4) than in acidic condition (pH 4.0). In PBS (phosphate buffered saline, pH 7.4), a higher initial burst release was observed, during which 80% of DOX was released within 3 h and 100% release of DOX was released after 77 h. In ABS (acetate buffer saline, pH 4), the initial burst release behavior was observed for the first 1 h with approximately 25.3% release of DOX. After then, the release of DOX slowed down and exhibited a sustained release after 10 h. The differences in the initial burst release behavior in pH 7.4 and 4.0 is presumably attributed to the different swelling ability of the INC filaments in these aqueous buffers (swelling ratio of 81.9±8% in pH 7.4 compared to swelling ratio of 20.3±6% in pH 4 after 10 min swelling, SI Figure S6).

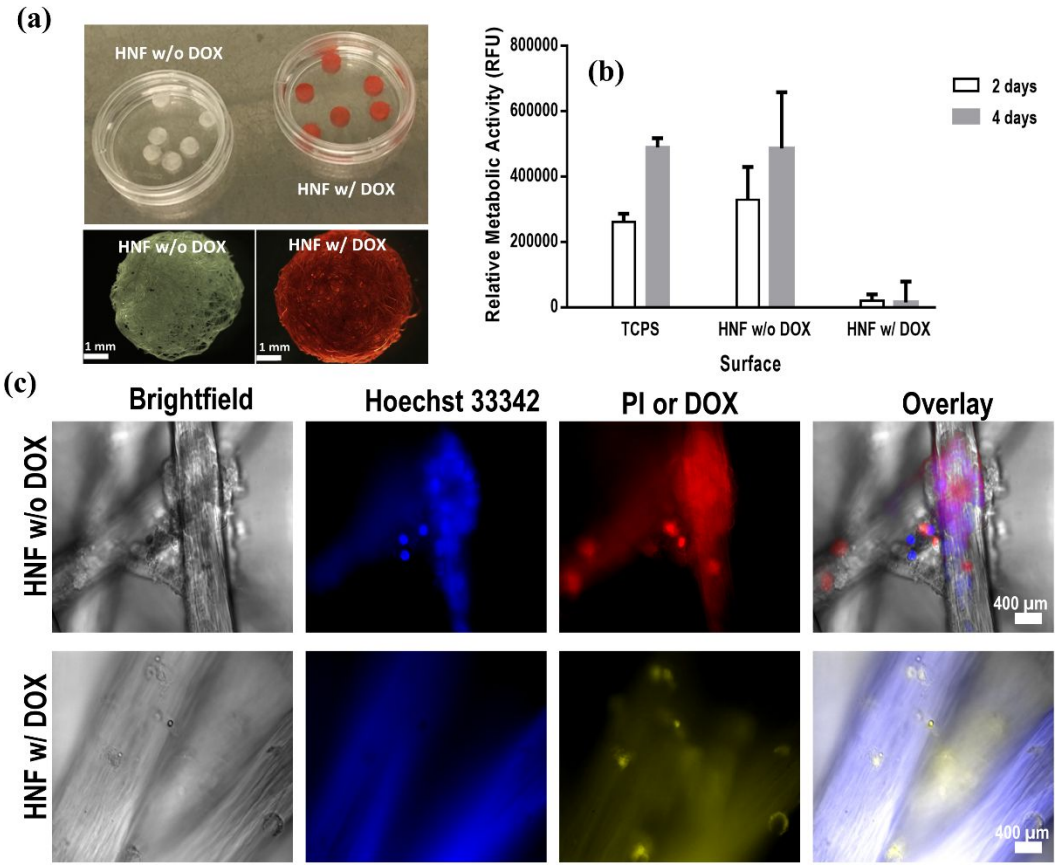

Figure 5. (a) Photography and optical microscopy images of hydro-entangled nanocellulose based INC filament scaffolds with (red, HNF w/ DOX) or without DOX (HNF w/o DOX). (b) Relative metabolic activity of NIH3T3 cells grown on HNF without DOX, with DOX, or on regular TCPS on 2 days (d2)

and 4 days (d4) post-seeding according to the Alamar Blue assay. (c) Fluorescence microscopic images of cell-laden HNF obtained on one day (d1) post-seeding. Cells on HNF w/o DOX was stained with Hoechst 33342 for live cells and PI for dead cells while cells on HNF w/DOX was stained only with Hoechst 33342.

An assessment of the cytotoxicity of NC based INC filaments with or without DOX was conducted to evaluate the suitability of NC based INC filament as biomaterials for drug delivery applications. Hydro-entangled nanocellulose based INC filament (HNF) scaffolds with or without DOX for cell culture by compressing six NC or DOX/NC based INC filaments (70 cm) using a hydro-entanglement process (Figure S8) were prepared. Entanglement of the filaments led to fibrous and porous scaffolds that retained excellent shape stability in water. Next, we examined the in vivo biocompatibilities of the HNFs for cell culture. Fibroblast NIH3T3 cells were seeded and cultured on the surfaces of the HNFs with a same seeding density. Figure 5b shows the effect of the surface type on cell growth (based on relative metabolic activity), which was measured on second (d2) and fourth (d4) day after initial seeding. Cells cultured on TCPS (tissue culture polystyrene) indicated significant growth from d2 to d4 with a two-tailed paired t-test showing $p < 0.01$. Growth was also detected on cells grown on HNF without DOX, albeit growth was not very statistically significant at $p = 0.06$. Although cell growth was slightly diminished, no significant cytotoxicity was observed, which is in line with previous reports on the cytotoxicity of nanocelluloses.[54-56] On the other hand, cells cultured on HNF with DOX did not show significant growth with paired t-test showing $p = 0.89$. This indicates that cells were mostly no longer metabolically active post d2 of culture, likely due to the cells internalizing DOX molecules that had been released from the scaffolds to the cell culture medium. When the relative metabolic activity is compared among the different surfaces at the same time point using the one-way ANOVA (analysis of variance), statistical significance is found only when comparing DOX-containing HNF against either HNF without DOX (p

< 0.05) or TCPS ($p < 0.01$). The relative metabolic activity was not significantly different for cells cultured on TCPS or HNF without DOX with $p = 0.32$ for the d2 time point and $p = 0.98$ for the d4 time point. This confirmed that the lack of growth of cells cultured on HNF with DOX was attributed to the presence of DOX. Significant release of DOX was also noticeable from the color of the medium that turned redder as the culture duration increased. Microscopic images of cells on HNF with and without DOX were also recorded on one day (d1) after seeding. As shown in Figure 5c, a cluster of cells can be observed attached on the HNF without DOX, which is a mixture of live (blue/Hoechst 33342) and dead (red/PI) cells. Note the detected autofluorescence from the HNF on both the blue and red channels. However, the stained nuclei were brighter, providing a relatively clear distinction against the HNF autofluorescence. On the HNF containing DOX, the majority of cells were not positively stained by Hoechst 33342, indicating that they were mostly dead or undergoing apoptosis.[57] Interestingly, the DOX fluorescence was detected brightly within the cells that did not stain positive for Hoechst; this indicates that the DOX had been internalized by cells, likely accumulating within the nuclei and inducing cell death. We demonstrated that nanocellulose based INC filaments could be used to encapsulate an antitumor drug molecule for pH responsive drug release and delivery, and hydro-entangled pure NC based INC filament scaffold had good biocompatibility towards cells. Unlike conventional nanocellulose based filament formation processes that involve toxic or acidic coagulation solvents, multi-steps and expensive equipment,[9, 58, 59] INC presents a simple, room-temperature, water-based process, allowing sensitive biological molecules such as proteins to be incorporated and continuously released from the NC based filaments with minimal loss of bioactivity. We believe NC based INC filaments could be further applied in tissue engineering such as 3D cell culture by incorporating cells and growth factors during the INC process.[52, 53, 60, 61]

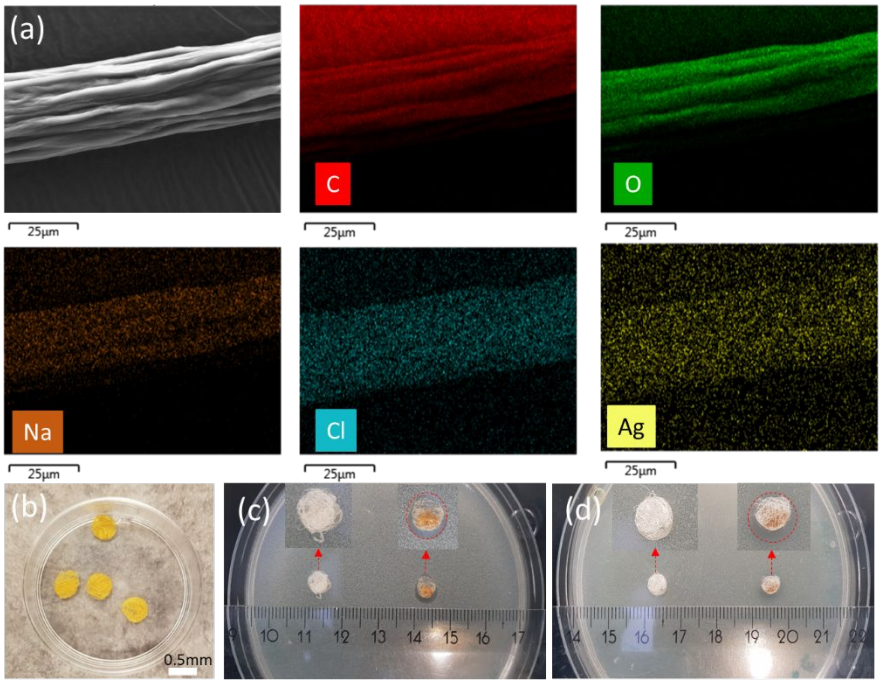

Figure 6. (a) View of energy dispersive spectroscopy (EDS) map of Ag NPs doped INC filaments; Photo of (b) disc fabric formed by five 70 cm Ag NPs doped INC filaments and the inhibition zone against (c) S.aureas and (d) E.coli.

Except hydrophilic molecule and hydrophobic nanomaterials, colloidal inorganic nanoparticles were also incorporated by INC process in this report. Ag (silver) NP (nanoparticle) was used as a colloidal inorganic nanoparticle model and the antimicrobial property of the formed Ag NPs/NC based INC filament was investigated. One droplet of 0.4 wt% TO-CNF suspension (100 μL) with 0.005 mmol/mL Ag NPs was used to draw the antimicrobial Ag NPs doped NC (Ag NPs/NC) based INC filament with another 100 μL droplet of 0.5 wt% AH-CNC (Figure 1d). The Ag NPs dispersion was stabilized by sodium citrate, which is negatively charged and prevents agglomeration of Ag nanoparticles. Citrate ions absorb on the surface of silver crystals to stabilize the silver particles.[62] We believe that it is the citrate facilitating the incorporation of Ag NPs in the formed filament. Figure 6a shows the view of energy dispersive spectroscopy (EDS) map of the resulting INC filament. It is observed that Ag element

distributed evenly on the surface of the formed filament, which successfully confirms the homogenous incorporation of Ag NPs. Moreover, sodium and chloride were also detected, which were probably formed by the complexation of the oppositely charged nanocellulose and then diffused onto the surface of the INC filaments. Ag NPs/NC based INC filaments disc (Figure 6b) was prepared by condensing five 70 cm filaments together via the same hydro-entanglement process. The antimicrobial property of the formed discs was tested against Gram-positive (*S.aureus*) and Gram-negative (*E.coli*) and pure nanocellulose INC filaments were used as a reference. After 24h incubation pristine nanocellulose based INC filaments did not show any antibacterial activity (inhibition zone) against tested microbial strains; however, antibacterial activity was observed with Ag NPs doped INC filaments towards both *S.aureas* and *E.coli* with slight loss of color. We envision that other colloidal inorganic nanoparitcles (e.g. gold NPs, see EDS map image in SI Figure S10) can also be incorporated into INC filaments to provide functional materials for various applications such as heterogeneous catalysis and biosensor.[63, 64]

CONCLUSIONS AND PERSPECTIVES

In summary, a new and simple technique to construct high-performance and functional macroscale fibers based on nanocellulose (NC) was developed. Nanocellulose based multifunctional filaments doped with carboxylated multi-walled carbon nanotubes (CMWCNTs), an antitumor drug (doxorubicin hydrochloride, DOX), and metal (silver) nanoparticles (Ag NPs) were successfully fabricated in aqueous circumstance at ambient temperature via interfacial nanoparticles complexation (INC). These nanostructured NC based filaments were demonstrated to possess great potential in wearable electronics, drug delivery, and antimicrobial materials applications. This straightforward and green approach based on the INC phenomenon not only offers unlimited freedom to design functional filaments since diverse chemical and biological materials (such as growth factors, cells and carbon nanomaterials) can be incorporated, but also provides possibilities for other charged nanoparticles and ribbons (e.g. charged

chitin nanofibers, graphene oxide, protein nanofibrils, etc) to construct new self-assembled filaments. We believe that there are vast uncharted areas that could be further exploited.

ASSOCIATED CONTENT

Supporting Information.

The Supporting Information is available free of charge on the ACS Publication website at DOI: xxx

Details of fabrication of cationic nanocellulose (AH-CNC) and anionic TO-CNF; details of fabrications of different nanocellulose (NC) based INC filaments; reaction mechanism of cationization of cellulose using sequential periodate oxidation and imidization with aminoguanidine hydrochloride for AH-CNC preparation; photos of INC filament drawing using tensile test machine; TEM images of positively charged AH-CNC and negatively charged TO-CNF; feasibility of filament drawing from the interface between adjacent droplets of AH-CNC and TO-CNF at various combinations of concentrations; SEM images of cross-section areas of pure nanocellulose based INC filaments; SEM images of cross-section area of CNTs/NC based INC filaments; optical images of water swelling of DOX/NC INC filaments in different pH for 10 min; schematic of the hydro-entanglement process; Energy Dispersive X-ray Spectroscopy (EDS) spectra of Ag NPs/NC INC filament.

AUTHOR INFORMATION

* Corresponding author: Henrikki Liimatainen

Email: Henrikki.Liimatainen@oulu.fi. Tel.: +358 8553 2416; Fax: +358 8553 2405.

Notes

There are no conflicts to declare.

ACKNOWLEDGEMENT

The authors acknowledge the support from the Academy of Finland project "Bionanochemicals" (298295) and European Regional Development Fund/Council of Oulu region ("Novidam" project). We also thank the support of Center of Microscopy and Nanotechnology in University of Oulu, Elisa Wirkkala for technical assistance in elemental analysis, Shu Hong for the help in photographing, Dr. Veli-Pekka Ronkainen for his help with fluorescence microscopy and Biocenter Finland for providing fluorescence microscopy facility used in this study.

ABBREVIATIONS

INC, interfacial nanoparticle complexation; NC, nanocellulose; AH-CNC, cationic aminoguanidine hydrochloride modified cellulose nanocrystal; TO-CNF, 2,2,6,6-tetramethylpiperidinyl-1-oxy radical (TEMPO) oxidized cellulose nanofibers; DOX, doxorubicin hydrochloride; CMWCNTs, carboxlyated multi-walled carbon nanotubes.

REFERENCES

(1) Meyers, M. A.; McKittrick, J.; Chen, P.-Y. Structural Biological Materials: Critical Mechanics-Materials Connections. *Science* **2013**, *339*, 773-779.

(2) Wegst, U. G. K.; Bai, H.; Saiz, E.; Tomsia, A. P.; Ritchie, R. O. Bioinspired Structural Materials. *Nature Materials* **2014**, *14*, 23-26.

(3) Goerlitzer, E. S. A.; Klupp Taylor, R. N.; Vogel, N. Bioinspired Photonic Pigments from Colloidal Self-Assembly. *Adv Mater* **2018**, *30*, 1706654.

(4) Zhao, N.; Wang, Z.; Cai, C.; Shen, H.; Liang, F.; Wang, D.; Wang, C.; Zhu, T.; Guo, J.; Wang, Y.; Liu, X.; Duan, C.; Wang, H.; Mao, Y.; Jia, X.; Dong, H.; Zhang, X.; Xu, J. Bioinspired Materials: from Low to High Dimensional Structure. *Adv Mater* **2014**, *26*, 6994-7017.

(5) Yang, Y.; Song, X.; Li, X.; Chen, Z.; Zhou, C.; Zhou, Q.; Chen, Y. Recent Progress in Biomimetic Additive Manufacturing Technology: From Materials to Functional Structures. *Adv Mater* **2018**, *30*, 1706539.

(6) Sun, H.; Luo, Q.; Hou, C.; Liu, J. Nanostructures Based on Protein Self-Assembly: From Hierarchical Construction to Bioinspired Materials. *Nano Today* **2017**, *14*, 16-41.

(7) Xiong, R.; Kim, H. S.; Zhang, S.; Kim, S.; Korolovych, V. F.; Ma, R.; Yingling, Y. G.; Lu, C.; Tsukruk, V. V. Template-Guided Assembly of Silk Fibroin on Cellulose Nanofibers for Robust Nanostructures with Ultrafast Water Transport. *Acs Nano* **2017**, *11*, 12008-12019.

(8) Mittal, N.; Jansson, R.; Widhe, M.; Benselfelt, T.; Håkansson, K. M. O.; Lundell, F.; Hedhammar, M.; Söderberg, L. D. Ultrastrong and Bioactive Nanostructured Bio-Based Composites. *Acs Nano* **2017**, *11*, 5148-5159.

(9) Mittal, N.; Ansari, F.; Gowda.V, K.; Brouzet, C.; Chen, P.; Larsson, P. T.; Roth, S. V.; Lundell, F.; Wågberg, L.; Kotov, N. A.; Söderberg, L. D. Multiscale Control of Nanocellulose Assembly: Transferring Remarkable Nanoscale Fibril Mechanics to Macroscale Fibers. *Acs Nano* **2018**, *12*, 6378-6388.

(10) Shang, L.; Yu, Y.; Liu, Y.; Chen, Z.; Kong, T.; Zhao, Y. Spinning and Applications of Bioinspired Fiber Systems. *Acs Nano* **2019**, *13*, 2749-2772.

(11) Moon, R. J.; Martini, A.; Nairn, J.; Simonsen, J.; Youngblood, J. Cellulose Nanomaterials Review: Structure, Properties and Nanocomposites. *Chem. Soc. Rev.* **2011**, *40*, 3941-3994.

(12) Klemm, D.; Cranston, E. D.; Fischer, D.; Gama, M.; Kedzior, S. A.; Kralisch, D.; Kramer, F.; Kondo, T.; Lindström, T.; Nietzsche, S.; Petzold-Welcke, K.; Rauchfuß, F. Nanocellulose as a Natural Source for Groundbreaking Applications in Materials Ccience: Today's State. *Mater Today* **2018**, *21*, 720-748.

(13) Tang, J. T.; Sisler, J.; Grishkewich, N.; Tam, K. C. Functionalization of Cellulose Nanocrystals for Advanced Applications. *J Colloid Interf Sci* **2017**, *494*, 397-409.

(14) Sirvio, J. A.; Visanko, M. Anionic Wood Nanofibers Produced from Unbleached Mechanical Pulp by Highly Efficient Chemical Modification. *J Mater Chem A* **2017**, *5*, 21828-21835.

(15) Liimatainen, H.; Visanko, M.; Sirviö, J. A.; Hormi, O. E. O.; Niinimaki, J. Enhancement of the Nanofibrillation of Wood Cellulose through Sequential Periodate-Chlorite Oxidation. *Biomacromolecules* **2012**, *13*, 1592-1597.

(16) Xiong, R.; Kim, H. S.; Zhang, L.; Korolovych, V. F.; Zhang, S.; Yingling, Y. G.; Tsukruk, V. V. Wrapping Nanocellulose Nets around Graphene Oxide Sheets. *Angew. Chem.* **2018**, *130*, 8644-8649.

(17) Zhu, C.; Monti, S.; Mathew, A. P. Cellulose Nanofiber–Graphene Oxide Biohybrids: Disclosing the Self-Assembly and Copper-Ion Adsorption Using Advanced Microscopy and ReaxFF Simulations. *Acs Nano* **2018**, *12*, 7028-7038.

(18) Salas, C.; Nypelö, T.; Rodriguez-Abreu, C.; Carrillo, C.; Rojas, O. J. Nanocellulose Properties and Applications in Colloids and Interfaces. *Current Opinion in Colloid & Interface Science* **2014**, *19*, 383-396.

(19) Lagerwall, J. P. F.; Schütz, C.; Salajkova, M.; Noh, J.; Hyun Park, J.; Scalia, G.; Bergström, L. Cellulose Nanocrystal-Based Materials: from Liquid Crystal Self-Assembly and Glass Formation to Multifunctional Thin Films. *Npg Asia Mater* **2014**, *6*, e80.

(20) Kontturi, E.; Laaksonen, P.; Linder, M. B.; Nonappa; Groschel, A. H.; Rojas, O. J.; Ikkala, O. Advanced Materials through Assembly of Nanocelluloses. *Adv Mater* **2018**, *30*, e1703779.

(21) Parker, R. M.; Frka-Petesic, B.; Guidetti, G.; Kamita, G.; Consani, G.; Abell, C.; Vignolini, S. Hierarchical Self-Assembly of Cellulose Nanocrystals in a Confined Geometry. *Acs Nano* **2016**, *10*, 8443-8449.

(22) Rofouie, P.; Alizadehgiashi, M.; Mundoor, H.; Smalyukh, I. I.; Kumacheva, E. Self-Assembly of Cellulose Nanocrystals into Semi-Spherical Photonic Cholesteric Films. *Adv Funct Mater* **2018**, *28*, 1803852.

(23) Tang, Z.; Wang, Y.; Podsiadlo, P.; Kotov, N. A. Biomedical Applications of Layer-by-Layer Assembly: From Biomimetics to Tissue Engineering. *Adv Mater* **2006**, *18*, 3203-3224.

(24) Zhang, W.; Zhao, Q.; Yuan, J. Porous Polyelectrolytes: The Interplay of Charge and Pores for New Functionalities. *Angew. Chem. Int. Ed.* **2018**, *57*, 6754-6773.

(25) Zhao, Q.; An, Q. F.; Ji, Y.; Qian, J.; Gao, C. Polyelectrolyte Complex Membranes for Pervaporation, Nanofiltration and Fuel Cell Applications. *J Membrane Sci* **2011**, *379*, 19-45.

(26) Insua, I.; Wilkinson, A.; Fernandez-Trillo, F. Polyion complex (PIC) particles: Preparation and biomedical applications. *Eur Polym J* **2016**, *81*, 198-215.

(27) Wang, Q.; Schlenoff, J. B. Single- and Multicompartment Hollow Polyelectrolyte Complex Microcapsules by One-Step Spraying. *Adv Mater* **2015**, *27*, 2077-2082.

(28) Qi, G.-B.; Gao, Y.-J.; Wang, L.; Wang, H. Self-Assembled Peptide-Based Nanomaterials for Biomedical Imaging and Therapy. *Adv Mater* **2018**, *30*, 1703444.

(29) Wan, A. C. A.; Cutiongco, M. F. A.; Tai, B. C. U.; Leong, M. F.; Lu, H. F.; Yim, E. K. F. Fibers by Interfacial Polyelectrolyte Complexation – Processes, Materials and Applications. *Mater Today* **2016**, *19*, 437-450.

(30) Wang, F.; Liu, Z.; Wang, B.; Feng, L.; Liu, L.; Lv, F.; Wang, Y.; Wang, S. Multi-Colored Fibers by Self-Assembly of DNA, Histone Proteins, and Cationic Conjugated Polymers. *Angew. Chem. Int. Ed.* **2014**, *53*, 424-428.

(31) Lai, Z.; Chen, Y.; Tan, C.; Zhang, X.; Zhang, H. Self-Assembly of Two-Dimensional Nanosheets into One-Dimensional Nanostructures. *Chem* **2016**, *1*, 59-77.

(32) Grande, R.; Trovatti, E.; Carvalho, A. J. F.; Gandini, A. Continuous Microfiber Drawing by Interfacial Charge Complexation between Anionic Cellulose Nanofibers and Cationic Chitosan. *J Mater Chem A* **2017**, *5*, 13098-13103.

(33) Zou, J.; Kim, F. Self-Assembly of Two-Dimensional Nanosheets Induced by Interfacial Polyionic Complexation. *Acs Nano* **2012**, *6*, 10606-10613.

(34) Nechyporchuk, O.; Bordes, R.; Köhnke, T. Wet Spinning of Flame-Retardant Cellulosic Fibers Supported by Interfacial Complexation of Cellulose Nanofibrils with Silica Nanoparticles. *Acs Appl Mater Inter* **2017**, *9*, 39069-39077.

(35) Johnston, A. P. R.; Cortez, C.; Angelatos, A. S.; Caruso, F. Layer-by-layer engineered capsules and their applications. *Current Opinion in Colloid & Interface Science* **2006**, *11*, 203-209.

(36) Yavvari, P. S.; Awasthi, A. K.; Sharma, A.; Bajaj, A.; Srivastava, A. Emerging Biomedical Applications of Polyaspartic Acid-Derived Biodegradable Polyelectrolytes and Polyelectrolyte Complexes. *J Mater Chem B* **2019**, *7*, 2102-2122.

(37) Tang, T.; Weng, T.; Jia, H.; Luo, S.; Xu, Y.; Li, L.; Zhang, P. Harnessing the Layer-by-Layer Assembly Technique to Design Biomaterials Vaccines for Immune Modulation in Translational Applications. *Biomaterials Science* **2019**, *7*, 715-732.

(38) De Geest, B. G.; De Koker, S.; Sukhorukov, G. B.; Kreft, O.; Parak, W. J.; Skirtach, A. G.; Demeester, J.; De Smedt, S. C.; Hennink, W. E. Polyelectrolyte Microcapsules for Biomedical Applications. *Soft Matter* **2009**, *5*, 282-291.

(39) Liu, X. Q.; Picart, C. Layer-by-Layer Assemblies for Cancer Treatment and Diagnosis. *Adv Mater* **2016**, *28*, 1295-1301.

(40) Li, L.-L.; An, H.-W.; Peng, B.; Zheng, R.; Wang, H. Self-Assembled Nanomaterials: Design Principles, The Nanostructural Effect, and their functional mechanisms as antimicrobial or detection agents. *Mater Horizons* **2019,** *6,* 1794-1811.

(41) Zhang, K.; Liimatainen, H. Hierarchical Assembly of Nanocellulose-Based Filaments by Interfacial Complexation. *Small* **2018**, *14*, 1801937.

(42) Li, P.; Sirviö, J. A.; Asante, B.; Liimatainen, H. Recyclable Deep Eutectic Solvent for the Production of Cationic Nanocelluloses. *Carbohyd Polym* **2018**, *199*, 219-227.

(43) Liimatainen, H.; Sirviö, J.; Haapala, A.; Hormi, O.; Niinimäki, J. Characterization of Highly Accessible Cellulose Microfibers Generated by Wet Stirred Media Milling. *Carbohyd Polym* **2011**, *83*, 2005-2010.

(44) Hajian, A.; Lindström, S. B.; Pettersson, T.; Hamedi, M. M.; Wågberg, L. Understanding the Dispersive Action of Nanocellulose for Carbon Nanomaterials. *Nano Lett.* **2017**, *17*, 1439-1447.

(45) Liu, Y.; Sun, B.; Li, J.; Cheng, D.; An, X.; Yang, B.; He, Z.; Lutes, R.; Khan, A.; Ni, Y. Aqueous Dispersion of Carbon Fibers and Expanded Graphite Stabilized from the Addition of Cellulose Nanocrystals to Produce Highly Conductive Cellulose Composites. *Acs Sustain Chem Eng* **2018**, *6*, 3291-3298.

(46) Li, Y.; Zhu, H.; Wang, Y.; Ray, U.; Zhu, S.; Dai, J.; Chen, C.; Fu, K.; Jang, S.-H.; Henderson, D.; Li, T.; Hu, L. Cellulose-Nanofiber-Enabled 3D Printing of a Carbon-Nanotube Microfiber Network. *Small Methods* **2017**, *1*, 1700222.

(47) Yao, J.; Ji, P.; Sheng, N.; Guan, F.; Zhang, M.; Wang, B.; Chen, S.; Wang, H. Hierarchical Core-Sheath Polypyrrole@Carbon Nanotube/Bacterial Cellulose Macrofibers with High Electrochemical Performance for All-Solid-State Supercapacitors. *Electrochim Acta* **2018**, *283*, 1578-1588.

(48) Hamedi, M. M.; Hajian, A.; Fall, A. B.; Håkansson, K.; Salajkova, M.; Lundell, F.; Wågberg, L.; Berglund, L. A. Highly Conducting, Strong Nanocomposites Based on Nanocellulose-Assisted Aqueous Dispersions of Single-Wall Carbon Nanotubes. *Acs Nano* **2014**, *8*, 2467-2476.

(49) Li, Y.; Zhu, H.; Shen, F.; Wan, J.; Lacey, S.; Fang, Z.; Dai, H.; Hu, L. Nanocellulose as Green Dispersant for Two-Dimensional Energy Materials. *Nano Energy* **2015**, *13*, 346-354.

(50) Wang, X.; Wu, P. Fluorinated Carbon Nanotube/Nanofibrillated Cellulose Composite Film with Enhanced Toughness, Superior Thermal Conductivity, and Electrical Insulation. *Acs Appl Mater Inter* **2018**, *10*, 34311-34321.

(51) Liao, I. C.; Wan, A. C. A.; Yim, E. K. F.; Leong, K. W. Controlled Release from Fibers of Polyelectrolyte Complexes. *J. Controlled Release* **2005**, *104*, 347-358.

(52) Leong, M. F.; Toh, J. K. C.; Du, C.; Narayanan, K.; Lu, H. F.; Lim, T. C.; Wan, A. C. A.; Ying, J. Y. Patterned Prevascularised Tissue Constructs by Assembly of Polyelectrolyte Hydrogel Fibres. *Nature Communications* **2013**, *4*, 2353.

(53) Tai, B. C. U.; Wan, A. C. A.; Ying, J. Y. Modified Polyelectrolyte Complex Fibrous Scaffold as a Matrix for 3D Cell Culture. *Biomaterials* **2010**, *31*, 5927-5935.

(54) Lopes, V. R.; Sanchez-Martinez, C.; Stromme, M.; Ferraz, N. In Vitro Biological Responses to Nanofibrillated Cellulose by Human Dermal, Lung and Immune Cells: Surface Chemistry Aspect. *Part Fibre Toxicol* **2017**, *14*, 1.

(55) Colombo, L.; Zoia, L.; Violatto, M. B.; Previdi, S.; Talamini, L.; Sitia, L.; Nicotra, F.; Orlandi, M.; Salmona, M.; Recordati, C.; Bigini, P.; La Ferla, B. Organ Distribution and Bone Tropism of Cellulose Nanocrystals in Living Mice. *Biomacromolecules* **2015**, *16*, 2862-2871.

(56) Hujaya, S. D.; Lorite, G. S.; Vainio, S. J.; Liimatainen, H. Polyion Complex Hydrogels from Chemically Modified Cellulose Nanofibrils: Structure-Function Relationship and Potential for Controlled and pH-Responsive Release of Doxorubicin. *Acta Biomater* **2018**, *75*, 346-357.

(57) Wang, S.; Konorev, E. A.; Kotamraju, S.; Joseph, J.; Kalivendi, S.; Kalyanaraman, B. Doxorubicin Induces Apoptosis in Normal and Tumor Cells via Distinctly Different Mechanisms: INTERMEDIACY OF H_2O_2- AND p53-DEPENDENT PATHWAYS. *Journal of Biological Chemistry* **2004**, *279*, 25535-25543.

(58) Lundahl, M. J.; Klar, V.; Ajdary, R.; Norberg, N.; Ago, M.; Cunha, A. G.; Rojas, O. J. Absorbent Filaments from Cellulose Nanofibril Hydrogels through Continuous Coaxial Wet Spinning. *ACS Appl Mater Interfaces* **2018**, *10*, 27287-27296.

(59) Siqueira, G.; Kokkinis, D.; Libanori, R.; Hausmann, M. K.; Gladman, A. S.; Neels, A.; Tingaut, P.; Zimmermann, T.; Lewis, J. A.; Studart, A. R. Cellulose Nanocrystal Inks for 3D Printing of Textured Cellular Architectures. *Adv Funct Mater* **2017**, *27*, 1604619.

(60) Wan, A. C. A.; Liao, I. C.; Yim, E. K. F.; Leong, K. W. Mechanism of Fiber Formation by Interfacial Polyelectrolyte Complexation. *Macromolecules* **2004**, *37*, 7019-7025.

(61) Raghothaman, D.; Leong, M. F.; Lim, T. C.; Toh, J. K. C.; Wan, A. C. A.; Yang, Z.; Lee, E. H. Engineering cell matrix interactions in assembled polyelectrolyte fiber hydrogels for mesenchymal stem cell chondrogenesis. *Biomaterials* **2014**, *35*, 2607-2616.

(62) Jiang, X. C.; Chen, C. Y.; Chen, W. M.; Yu, A. B. Role of Citric Acid in the Formation of Silver Nanoplates through a Synergistic Reduction Approach. *Langmuir* **2010**, *26*, 4400-4408.

(63) Das, J.; Aziz, M. A.; Yang, H. A Nanocatalyst-Based Assay for Proteins: DNA-Free Ultrasensitive Electrochemical Detection Using Catalytic Reduction of p-Nitrophenol by Gold-Nanoparticle Labels. *J. Am. Chem. Soc.* **2006**, *128,* 16022-16023.

(64) Baranes, K.; Shevach, M.; Shefi, O.; Dvir, T. Gold Nanoparticle-Decorated Scaffolds Promote Neuronal Differentiation and Maturation. *Nano Lett.* **2016**, *16*, 2916-2920.

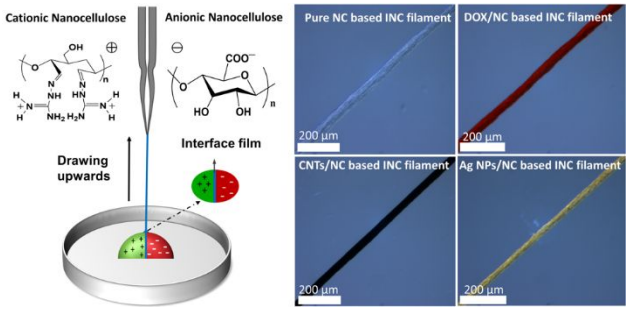
Cationic Nanocellulose
Anionic Nanocellulose
Drawing upwards
Interface film
Pure NC based INC filament
DOX/NC based INC filament
CNTs/NC based INC filament
Ag NPs/NC based INC filament
200 µm
200 µm
200 µm
200 µm

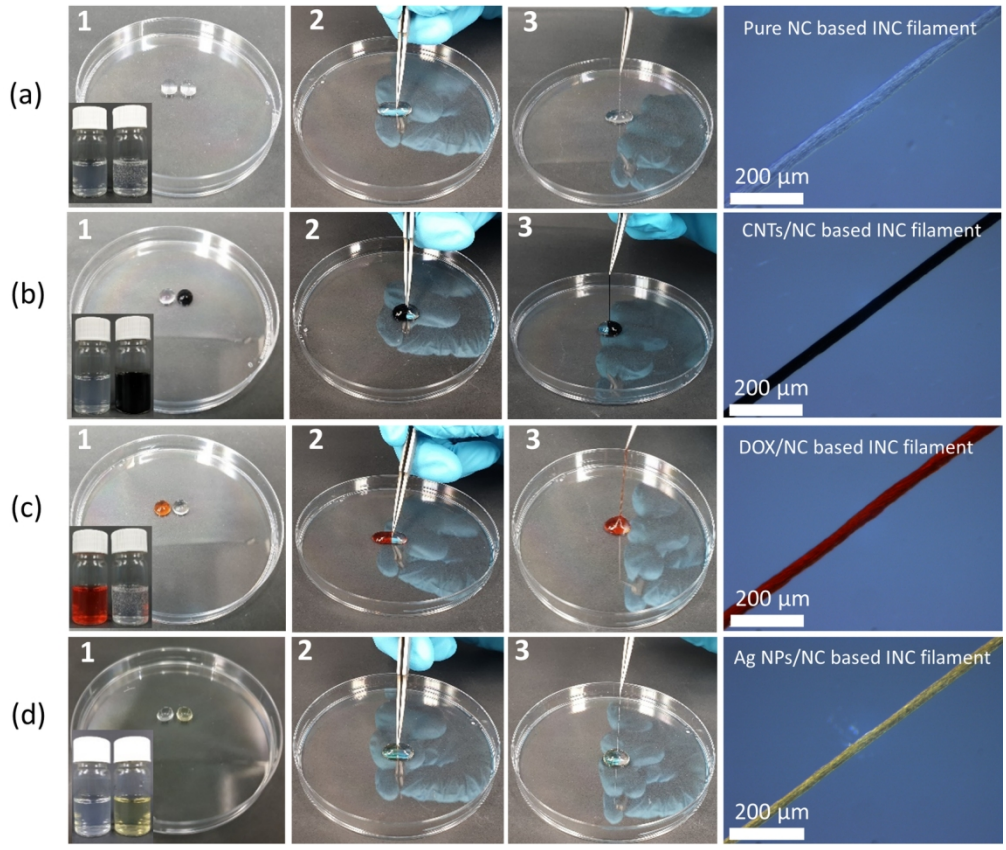

Figure 1. Digital photographs of the drawing process of each INC filament and corresponding optical microscope images of the dried INC filaments: (a) anionic suspension: 0.5 wt% TO-CNF; cationic suspension: 0.5 wt% AH-CNC; (b) anionic suspension: 0.5 wt% TO-CNF with 0.2 wt% CMWCNTs; cationic suspension: 0.5 wt% AH-CNC; (c) anionic suspension: 0.5 wt% TO-CNF; cationic suspension: 0.5 wt% AH-CNC with 200 µg/mL DOX; (d) anionic suspension: 0.4 wt% TO-CNF with 0.005 mmol/mL Ag NPs; cationic suspension: 0.5 wt% AH-CNC.

144x121mm (300 x 300 DPI)

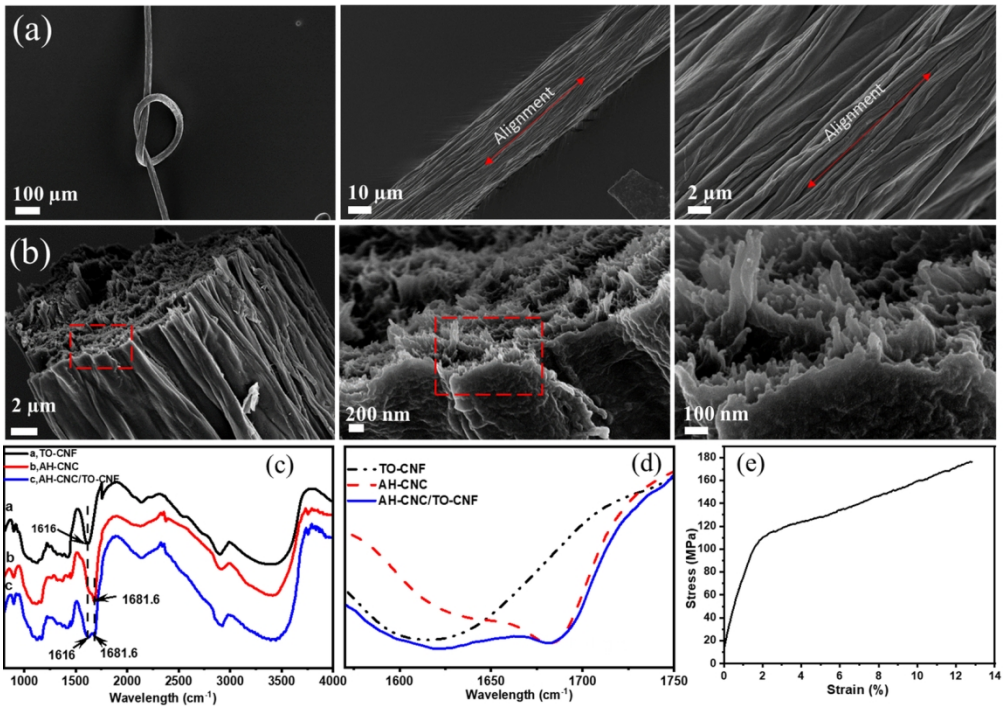

Figure 2. Scanning electron microscopy (SEM) images of (a) longitudinal direction and (b) cross-sectional fracture of pure nanocellulose based INC filaments. The DRIFT spectra (c) and typical peaks (d) of the formed pure nanocellulose based INC filaments and its respective components; (e) a typical stress-strain curve of the fabricated filaments using 0.5% TO-CNF and 0.5% AH-CNC.

142x99mm (300 x 300 DPI)

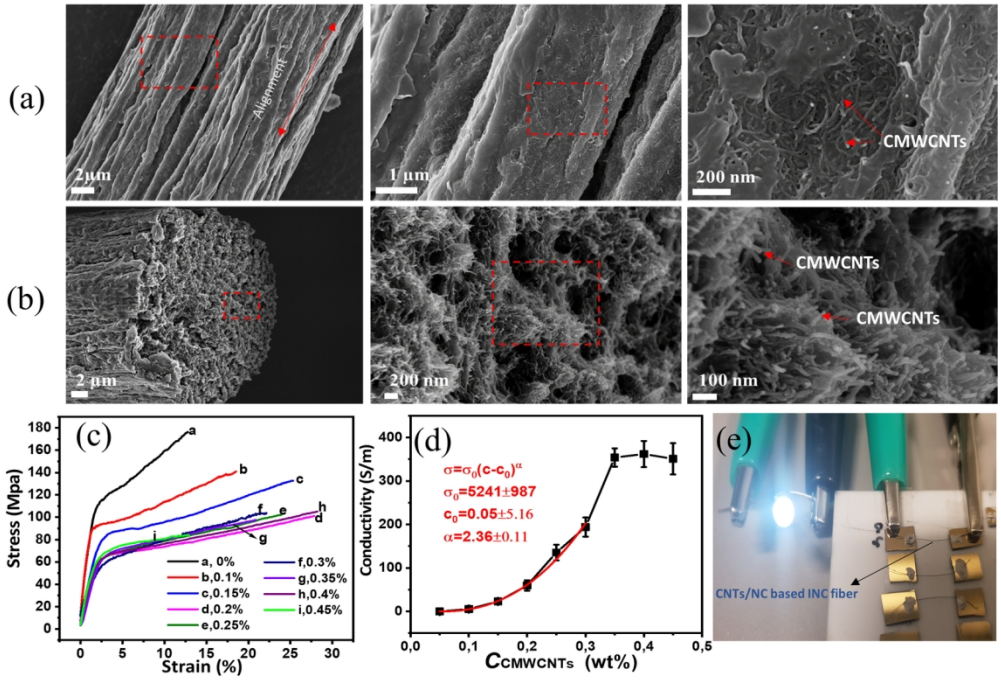

Figure 3. SEM images of (a) longitudinal and (b) cross-sectional fracture of CMWCNTs incorporated INC filaments. (c) Typical stress-strain curves and (d) electrical conductivity of INC filaments fabricated using different CMWCNTs concentrations in TO-CNF dispersion. (e) Photograph showing a light emitting diode (LED) operating using an individual CMWCNTs incorporated INC filament fabricated by 0.35 wt% CMWCNTs in TO-CNF suspension (47.3 wt% CMWCNTs, 45.5 μm diameter).

139x95mm (300 x 300 DPI)

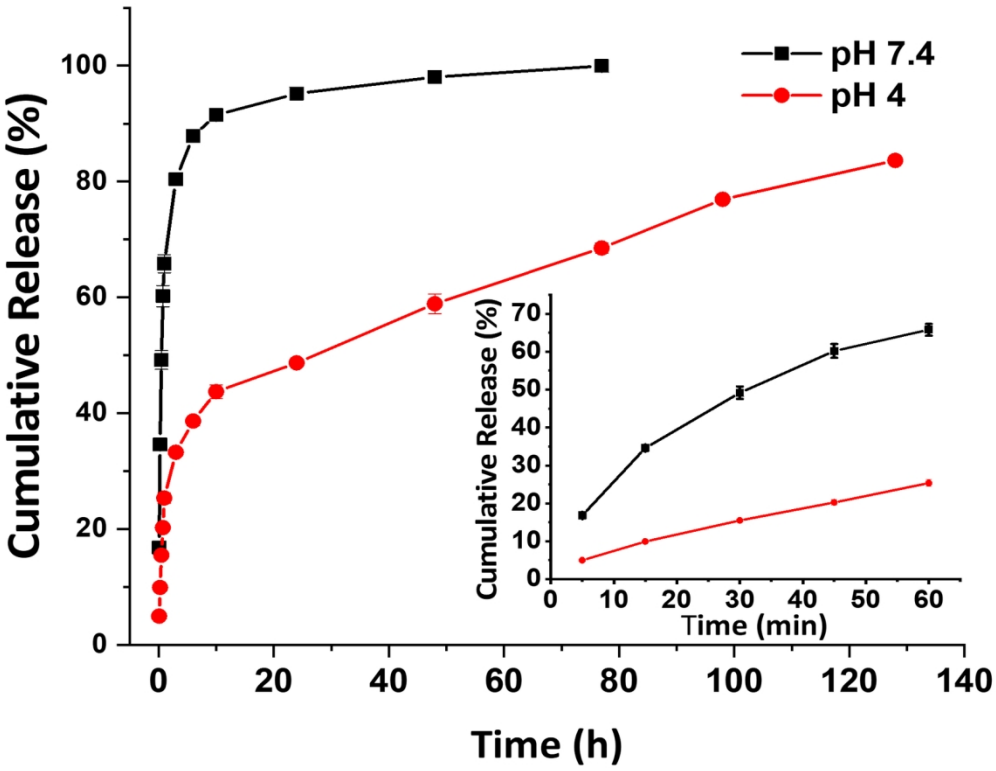

Figure 4. Cumulative release profiles of DOX-loaded NC based INC filaments in different pH values at 37 oC. The inset shows the cumulative drug release in the first one hour.

74x57mm (600 x 600 DPI)

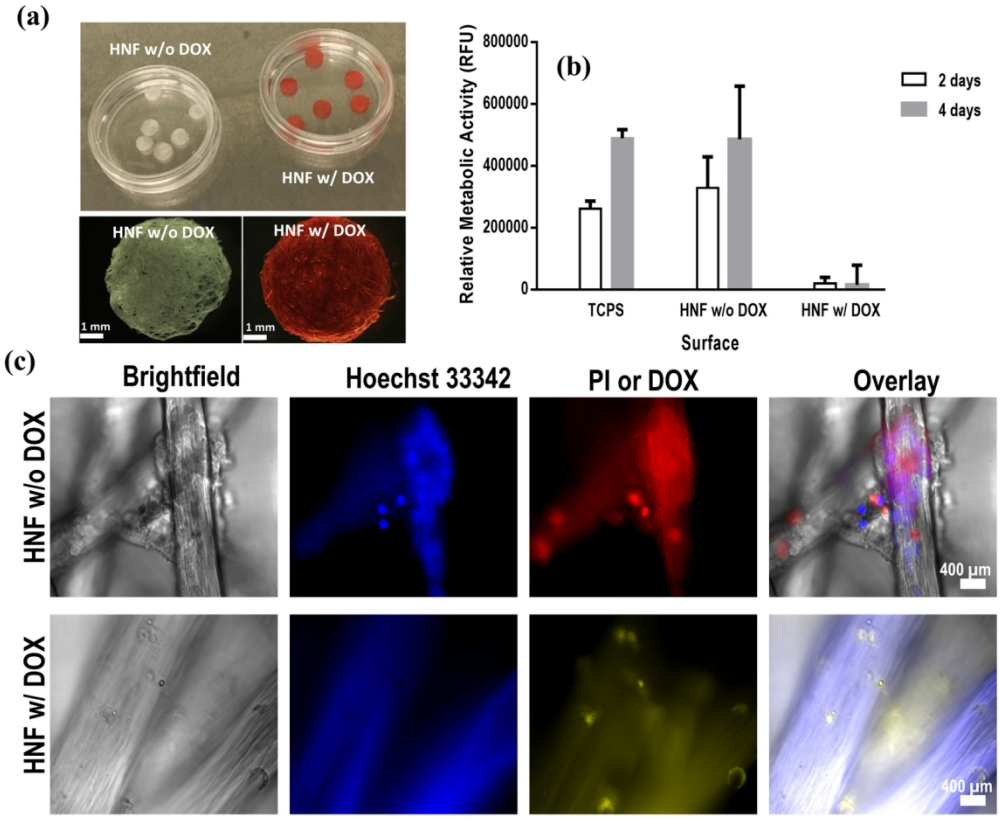

Figure 5. (a) Photography and optical microscopy images of hydro-entangled nanocellulose based INC filament scaffolds with (red, HNF w/ DOX) or without DOX (HNF w/o DOX). (b) Relative metabolic activity of NIH3T3 cells grown on HNF without DOX, with DOX, or on regular TCPS on 2 days (d2) and 4 days (d4) post-seeding according to the Alamar Blue assay. (c) Fluorescence microscopic images of cell-laden HNF obtained on one day (d1) post-seeding. Cells on HNF w/o DOX was stained with Hoechst 33342 for live cells and PI for dead cells while cells on HNF w/DOX was stained only with Hoechst 33342.

139x114mm (300 x 300 DPI)

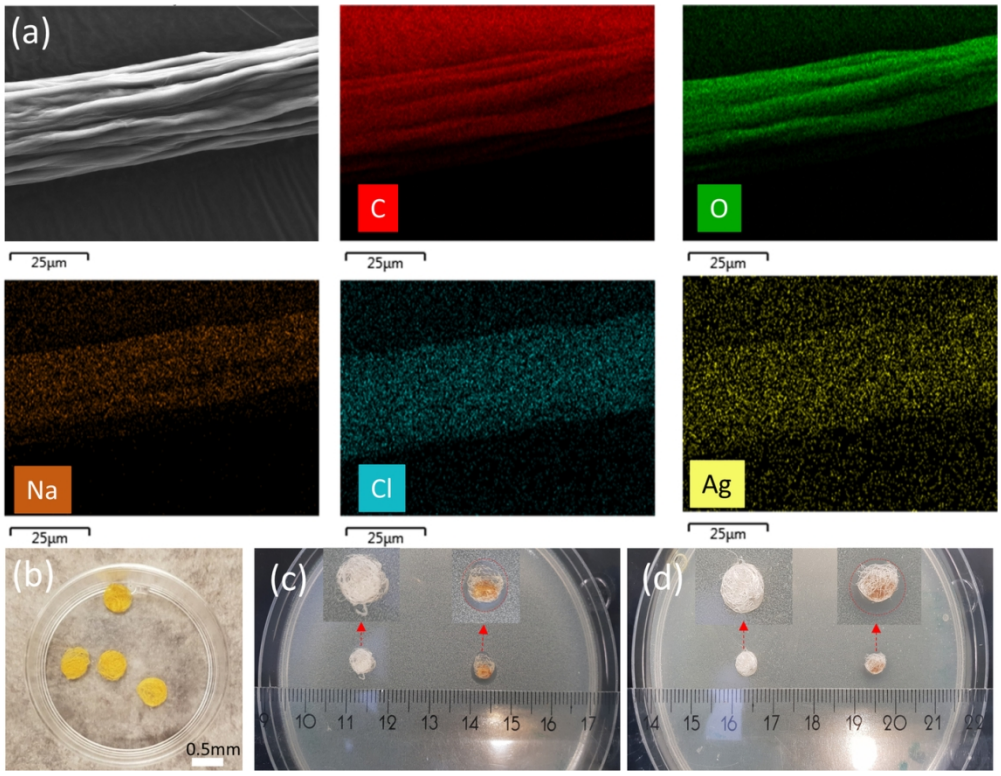

Figure 6. (a) View of energy dispersive spectroscopy (EDS) map of Ag NPs doped INC filaments; Photo of (b) disc fabric formed by five 70 cm Ag NPs doped INC filaments and the inhibition zone against (c) S.aureas and (d) E.coli.

119x91mm (300 x 300 DPI)